Analysis of Seismic Reduction Effect of U-Shaped Rubber Composite Isolation Bearing in Reticulated Shell Structure

Liu Yi
Beijing University of Technology, Beijing, China

Abstract: Long-span latticed shell structures are widely used in public buildings such as stadiums and transportation hubs due to their advantages of light weight, high strength, and flexible spatial forms. However, their complex response characteristics under dynamic loads such as earthquakes pose significant seismic safety hazards. To investigate the shock absorption effect of the proposed U-shaped composite damper and reduce the seismic response of latticed shell structures, a U-shaped rubber composite bearing (formed by combining the U-shaped composite damper with a lead-zinc rubber bearing) was applied to the latticed shell structure for nonlinear dynamic time-history analysis.

Keywords: U-Shaped Rubber Composite Isolation Bearing; Dynamic Time-History Analysis; Isolated Latticed Shell Structure

1. Introduction

Large-span spatial structures, with their spacious indoor spaces and flexible functional layouts, have been widely applied in modern public buildings. These structures not only meet the spatial scale and functional requirements of large public buildings such as sports venues, conference and exhibition centers, cultural and entertainment facilities, and airport terminals but also create unique architectural aesthetic effects. However, due to the special nature of their structural systems, large-span spatial structures often face severe safety challenges when encountering extreme disasters like fires and earthquakes [1]. Moreover, because of their large spans and light weight, these structures often suffer from insufficient stiffness, posing a risk of collapse under seismic loads [2]. Therefore, experts have conducted research on seismic isolation techniques for spatial structures, which mainly focuses on the following two aspects:

Replace the damping elements of large-span spatial structures with larger members or add additional members. Ma Jinfeng [3] proposed using viscoelastic dampers to replace the braces in cable-supported domes to reduce seismic response, and conducted parameter analysis on structural span, structural vector span ratio, damper parameters, and types of replaced members. Zhao Xiang [4] et al., based on the superelastic properties of shape memory alloys, successfully developed a multifunctional composite damper that integrates self-resetting, high energy dissipation, and amplification functions; the research team used a planar tetrahedral truss as the subject of study, employing the method of replacing some structural members with dampers to systematically analyze the vibration control effects of the device. Zhuang Peng [5] innovatively proposed a friction-SMA spring composite energy dissipation device, which was arranged at the column base and mid-span of the ring beam through pin nodes, forming an inverted V-shaped energy dissipation support system (FSB), providing new ideas for structural energy dissipation. Zhu Limin [6], focusing on the characteristics of large-span spatial structures, developed a lightweight buckling-restrained support system suitable for tree-like columns, established corresponding calculation models and design methods, significantly enhancing the seismic performance of the structure.

To reduce seismic response, seismic isolation bearings are arranged. Ma Yongquan [7], using the physical string-supported dome roof in Weifang as an engineering background, compared and analyzed the seismic responses of uncontrolled and isolated roofs, proving the effectiveness of SMA composite rubber bearings in reducing the seismic response of roofs. In recent years, scholars have conducted in-depth research on the application of friction pendulum bearings in spherical reticulated shell structures. Xue [8] et al. systematically studied changes in the design parameters of friction pendulum

bearings, revealing their effects on the seismic response of spherical reticulated shell structures. Zhuang Peng [9] et al. innovatively proposed a multi-functional friction pendulum bearing (MFPB) and applied it to the seismic isolation system of single-layer spherical reticulated shell structures; through nonlinear time-history analysis, they compared the dynamic response indicators of the reticulated shell structure under controlled and uncontrolled conditions, verifying the effectiveness of this seismic isolation system. Kong [10] et al. focused on the impact of support column parameters on seismic performance, systematically analyzing the correlation between support column height and cross-sectional area with seismic isolation effects. To enhance the energy dissipation capability of the bearing, Zhang [11] et al. formed vertical seismic isolation bearings by paralleling springs and viscous dampers, and transformed triple friction pendulum bearings into horizontal seismic isolation bearings, studying the influence of three-dimensional seismic isolation bearings on the seismic isolation effect of reticulated shell structures. Zhu Zhaochen [12] et al. designed a multi-frequency mass damper (MTMD) vibration reduction device and conducted K6-type single-layer spherical reticulated shell MTMD vibration control test bench experiments.

Therefore, three finite element models were established: the grid shell uncontrolled structure, the U-shaped rubber composite seismic isolation structure, and the lead-core rubber seismic isolation structure. Next, the natural frequencies and periods of these three structures were analyzed and compared. Additionally, the seismic isolation effects of the U-shaped rubber composite seismic isolation structure and the lead-core rubber seismic isolation structure were compared, analyzing the reduction rates of key node displacements, accelerations, and internal forces in members under El centro, Taft, and 1979 seismic waves in three directions. Finally, the reduction rates of key node displacements, accelerations, and internal forces in members under 0.2g and 0.4g seismic intensities for the U-shaped rubber composite seismic isolation structure were compared to further determine the applicable conditions for the U-shaped rubber composite seismic isolation bearings.

2. The Model of Single-Layer Net Shell Seismic Isolation Structure Is Established

The model of K6 single-layer reticulated shell is established. The single-layer spherical grid shell structure system, especially the K6 type Kuwaiti system, has become an important research subject in the field of spatial structures due to its optimized geometric configuration, symmetrical mesh division, and superior mechanical properties. This system not only possesses a complete numerical modeling theory but is also widely used as a benchmark model for large-span space structure research due to its typical structural characteristics. Existing literature has conducted multidimensional studies on such structures, including but not limited to the mechanisms of elastoplastic instability, internal force analysis theory, and initial bending effects, among other key mechanical issues.

Based on the above research background and technical characteristics, this study selected the structural form of a KW-K6 type single-layer spherical grid shell with a span of 60m for seismic isolation bearing application research. The structural parameter design strictly adhered to current design standards and combined with practical engineering experience. The determination of the grid shell design parameters is shown in Table 1, and the plan and elevation drawings are shown in Figure 1.

Table 1. Design Parameter Values of K6 Single-Layer Spherical Latticed Shell

span	Frequency of division	ratio of rise to span	Outer diameter of section of member / mm	Wall thickness of member / mm
60	6	1/5	180	6

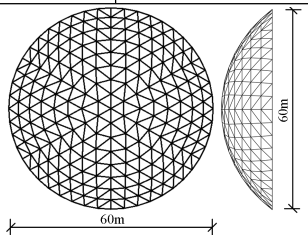

Figure 1. Modular Assembled K6 Reticulated Shell

The finite element model of KW-K6 vertical shell structure is constructed by Abaqus finite element software. In this model, the member unit adopts B31 beam unit, and the material constitutive model selects Q345 steel. The material properties are shown in Figure 2.

Support model is established

The four U-shaped composite dampers obtained from the second chapter are combined with lead

rubber bearings (LRB400) to form a U-shaped rubber composite seismic isolation bearing, which is installed at the bottom of the reticulated shell, as shown in Figure 3. The red-marked points indicate the positions where the seismic isolation bearings are arranged, with a total of 48 seismic isolation bearings arranged in the structure. The mechanical performance parameters of the seismic isolation bearings used in this chapter are listed in Table 2 In actual engineering applications, the bearing parameters can be repeatedly optimized to achieve the ideal seismic isolation bearing parameter values for the system.

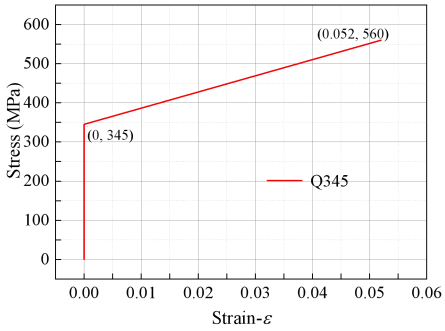

Figure 2. Constitutive Relation Model of Q345 Steel

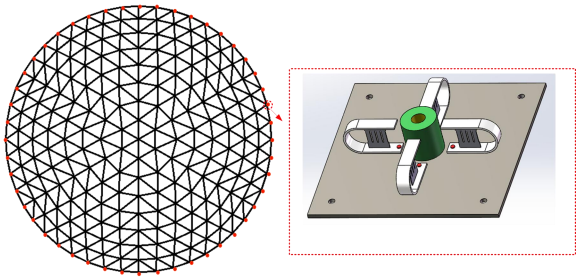

Figure 3. Layout Plan of the Isolation Bearings for the Latticed Shell

D refers to the effective diameter of the lead rubber bearing, d refers to the lead diameter of the lead rubber bearing, and ts refers to the total thickness of the rubber layer of the lead rubber bearing.

Verification of simplified model of seismic isolation bearings

This chapter focuses on the mechanism of seismic isolation devices affecting the dynamic characteristics of spatial reticulated shell structures. By establishing a comparative analysis system between seismic isolation bearings and non-seismic isolation bearing reticulated shell structures, it analyzes the vibration reduction effect of seismic isolation bearings on reticulated shell structures. During numerical simulation, to improve computational resource utilization efficiency and accurately reflect the mechanical properties of seismic isolation devices, a Cartesian connector (Cartesian connector) from the Abaqus connector library is used to construct a three-dimensional equivalent model of the seismic isolation device. The "Cartesian" connection determines the motion components between two points by measuring the coordinate changes in three connection directions relative to one point, without adding any motion constraints, which increases computational efficiency for simulating three-dimensional seismic isolation bearings [13]. To verify whether the simplified seismic isolation bearing connection units meet the accuracy requirements, numerical simulations were conducted on simplified models of seismic isolation bearings using both connector units and solids.

Table 2. Table of Parameter Changes of Shock Absorbing Bearings

tu/mm	ru/mm	bu/mm	rc/mm	hc/mm	nc/mm	bc/mm	tc/mm	D/mm	d/mm	ts/mm
15	130	100	4	130	4	40	4	400	160	156

As shown in Figure 4, the load-displacement curves obtained from both models are very close. In the early loading stage, when the rotation angle is less than 0.05 radians, the stiffness of the seismic isolation bearing connector model is very close to that of the solid element model. When the rotation angle exceeds 0.05 radians, the stiffness of the seismic isolation bearing connector model is slightly less than that of the solid element model. Therefore, the connector model can be used instead of the solid element model for nonlinear time-history analysis of reticulated shell seismic isolation structures.

Analysis steps and boundary condition setting

In ABAQUS, set up three analysis steps for the dynamic time-history analysis of the reticulated shell model. The first step is the initial step, used to set the initial boundary conditions; the second step is the static analysis step, used to apply gravity to the reticulated shell structure to more accurately reflect its true state; the third step sets up the dynamic analysis step, where three-dimensional seismic waves are input.

During the structural dynamic response analysis process, boundary conditions should be adjusted according to different stages of analysis. For seismic isolation systems, in the initial and static analysis phases, all six degrees of freedom of the seismic isolation bearings must be constrained; when entering the dynamic analysis phase, to

account for the impact of earthquakes, the translational degrees of freedom in the X, Y, and Z directions of the seismic isolation bearings need to be released. Correspondingly, for non-seismic isolation systems, in the initial and static analysis phases, the six degrees of freedom at the bottom nodes of the reticulated shell structure should be fully constrained; however, during the dynamic analysis phase, the translational degrees of freedom in the three translational directions at the bottom nodes should be released to accurately simulate the dynamic response characteristics of the structure under earthquake action.

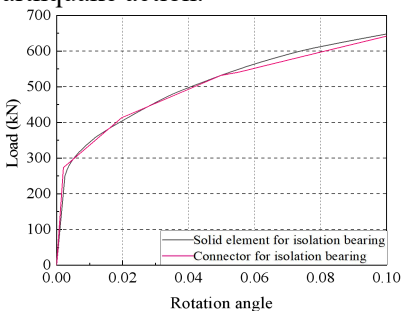

Figure 4. Verification of the Simplified Model

Mesh structure damping setting

This paper analyzes the use of Rely damping (Rayleigh) method for setting up damping in reticulated shell structures. The Rely damping method determines the structure's damping matrix through the combination of mass and stiffness matrices. The central frequency of Rely damping is determined using the natural frequency, which involves performing undamped natural frequency calculations on the model to determine the frequency. This paper extracts the first two natural frequencies for Rely damping calculations, with the formula as follows:

$$\alpha = \frac{4\pi f_1 f_2 \xi}{f_1 + f_2} \quad (1)$$

$$\beta = \frac{\xi}{\pi(f_1 + f_2)} \quad (2)$$

F1 is the first order frequency of the structure, f2 is the second ξ order frequency of the structure, and the damping ratio of the structure is 0.02.

3. Seismic Waves and the Selection of Key Nodes and Members

Select El centro, Taft, and 1979 seismic waves to conduct nonlinear time-history analysis on different types of base isolation bearings and structural systems with varying levels of seismic intensity. Scale the peak ground acceleration (Peak ground acceleration, hereafter referred to as PGA) from each seismic record to 0.2g and 0.40g, and input them in the ratio of 1 (X-direction): 0.85 (Y-direction): 0.65 (Z-direction). This yields the peak acceleration and displacement responses at critical nodes of the reticulated shell structure, as well as the internal forces in key members. Define the critical displacement nodes, critical acceleration nodes, and critical members of the reticulated shell structure as follows:

Under the action of El centro-wave, key displacement nodes are defined as Node 33 (X-direction), 130 (Y-direction), and 3 (Z-direction); key acceleration nodes are defined as Node 36 (X-direction), 6 (Y-direction), and 26 (Z-direction); and key members are defined as Member 1. Under the action of Taft wave, key displacement nodes are defined as Node 164 (X-direction), 52 (Y-direction), and 8 (Z-direction); key acceleration nodes are defined as Node 132 (X-direction), 197 (Y-direction), and 129 (Z-direction); and key members are defined as Member 2. Under the action of the 1979 wave, key displacement nodes are defined as Node 183 (X-direction), 50 (Y-direction), and 3 (Z-direction); key acceleration nodes are defined as Node 3 (X-direction), 4 (Y-direction), and 130 (Z-direction); and key members are defined as Member 3, as shown in Figure 5.

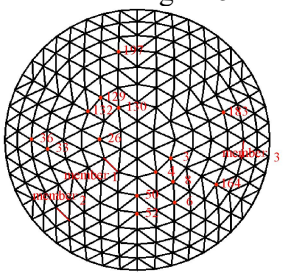

Figure 5. Key Nodes and Members Diagram of Latticed Shell

The seismic response and damping rate of the defined shell structure are as follows:

$$\varepsilon = \frac{\text{Maximum dynamic response of non-isolated structures} - \text{Maximum dynamic response of isolated structures}}{\text{Maximum dynamic response of non-isolated structures}} \times 100\% \quad (3)$$

4. Self-Oscillation Analysis of the Net Shell

The analysis of the self-vibration characteristics of structures primarily aims to determine the natural frequencies of the structure or its components, which also serves as the foundation for further dynamic analysis. By conducting self-vibration analyses on the unseismic

reticulated shell structure M1, the seismic-retained reticulated shell structure M2 with U-shaped rubber composite seismic isolation bearings, and the seismic-retained reticulated shell structure M3 with lead-core rubber bearings, we obtained the first ten modes and periods for each, as shown in Table 3.

Table 3. The First 10 Natural Frequencies and Periods of the Latticed Shell Model

order	model M1		model M2		model M3	
	frequency (HZ)	period (s)	frequency (HZ)	period (s)	frequency (HZ)	period (s)
1	4.90	0.20	0.74	1.35	1.58	0.63
2	4.90	0.20	1.61	0.62	1.84	0.54
3	5.41	0.18	1.90	0.52	3.53	0.28
4	5.46	0.18	3.54	0.28	4.17	0.24
5	5.46	0.18	4.18	0.24	4.32	0.23
6	5.51	0.18	4.33	0.24	4.60	0.22
7	5.51	0.18	4.62	0.22	4.65	0.22
8	5.67	0.18	4.67	0.21	4.95	0.20
9	5.67	0.18	4.96	0.20	5.05	0.20
10	5.74	0.17	5.10	0.20	5.32	0.19

From this, it can be seen that the first ten natural vibration periods of the cable-supported dome structure with seismic isolation bearings are significantly longer than those of the uncontrolled structure. The first period of the cable-supported dome structure with lead rubber bearings (M3) is 0.63 seconds, which is 3.15 times that of the uncontrolled structure, and the increase in natural frequency after the third period is slightly more pronounced; the first period of the cable-supported dome structure with U-shaped rubber composite seismic isolation bearings is 1.35 seconds, which is 6.75 times that of the uncontrolled structure's first period and 2.14 times that of the cable-supported dome structure with lead rubber bearings, and the increase in natural frequency after the fourth period is somewhat more significant. It is evident that setting up seismic isolation bearings alters the dynamic characteristics of the structure, making its natural vibration periods avoid the excellent periods of seismic waves to prevent resonance reactions, while also extending the natural vibration periods, effectively reducing the seismic response of the cable-supported dome structure.

5. Analysis of the Optimal Seismic Isolation Effect of U-shaped Rubber Composite Seismic Isolation Bearing

Comparison and analysis of key node displacement

The comparative analysis of the seismic response under the action of a 0.4g earthquake wave shows that the node displacement reduction effect is better when using U-shaped rubber composite base bearings and lead-core rubber bearings. Figure 6 presents the key nodal displacement time-history curves in three directions for the U-shaped rubber composite base shell structure and the lead-core rubber base shell structure during the El centro, Taft, and 1979 earthquake waves. Figure 7 provides the peak nodal displacements in three directions under the action of the three types of earthquake waves. Table 4 lists the damping ratios of the U-shaped rubber composite base bearing and the lead-core rubber bearing. It can be seen from these results:

U-shaped rubber composite seismic isolation bearings and lead-core rubber bearings both effectively reduce the dynamic response of structures, but their seismic isolation effects differ. Specifically, both types of seismic isolation bearings have vibration reduction effects on the peak nodal displacements of reticulated shell structures. Under El centro-waves, the vibration reduction rates in the X, Y, and Z directions for U-shaped rubber composite seismic isolation bearings are 49.7%,37.9%, and 53.9%, respectively; under Taft waves, they are 59.6%,59.5%, and 62.6%; under 1979 waves, they are 51.8%,49.9%, and 61.4%. Under lead-core rubber bearings, the vibration reduction rates in the X, Y, and Z directions are 13.4%,15.8%, and 19.4%, respectively; under Taft waves, they are 29.4%,19.5%, and 35.7%; under 1979 waves, they are 20.4%,25.3%, and 30.8%.

Under the three types of seismic waves, the peak nodal displacements in the Z direction for both uncontrolled and controlled structures are greater than those in the X and Y directions. Compared to the non-seismic isolation grid shell

structure, the horizontal damping rate of the two seismic isolation grid shell structures is lower than their vertical damping rate. The seismic isolation bearings show significant damping under the Taft wave and the 1979 wave. For grid shell structures, these seismic wave spectral characteristics lead to displacement, causing the seismic isolation bearings to enter the plastic stage earlier and dissipate more energy.

Compared to the lead-core rubber bearing, the displacement damping rate under El centro-wave is 22.1%-36.3% lower, under Taft wave it is 26.9%-40% lower, and under 1979 wave it is 19.6%-31.4% lower. It can be seen that there is a significant difference in the displacement damping effect between the two. This is because, compared to the lead-core rubber bearing, the U-shaped rubber composite seismic isolation bearing increases stiffness and energy dissipation capacity, allowing the U-shaped rubber composite damper to enter plasticity and fully dissipate energy under a 0.4g earthquake intensity.

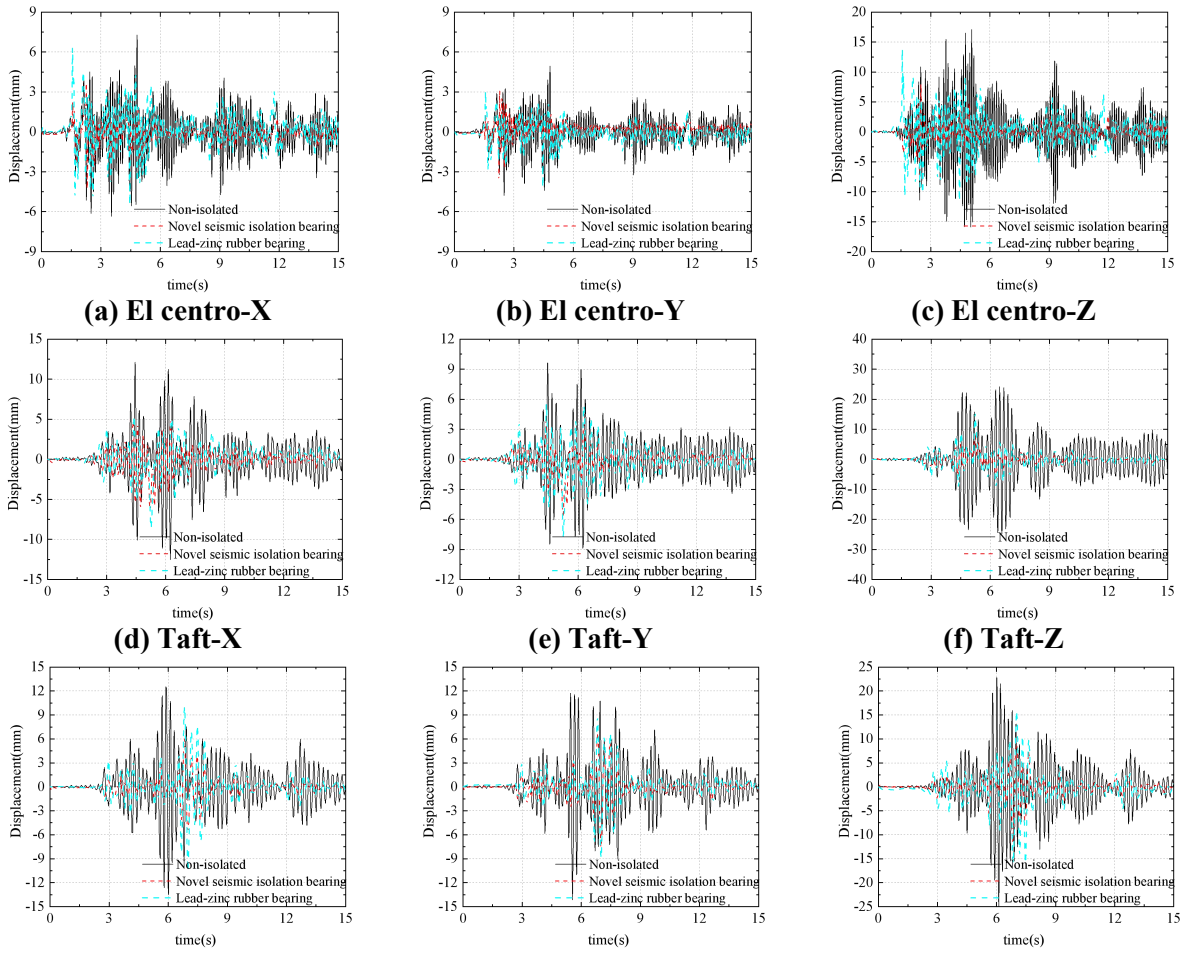

(a) El centro-X (b) El centro-Y (c) El centro-Z

(d) Taft-X (e) Taft-Y (f) Taft-Z

(g) 1979-X (h) 1979-Y (i) 1979-Z

Figure 6. Displacement Time History Curve of Key Nodes of the Latticed Shell Structure under the Action of 0.4PGA Seismic Wave

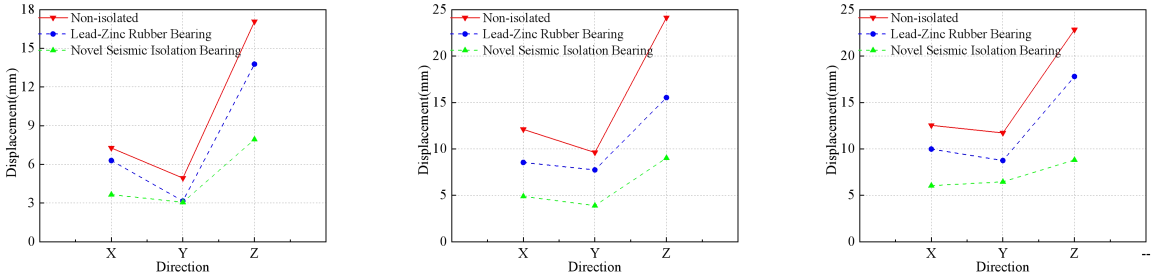

(a) El centro (b) Taft (c) 1979

Figure 7. Peak Displacement of Key Nodes of the Latticed Shell Structure under the Action of 0.4PGA Seismic Wave

Table 4. Comparison of the Shock Absorption Rates of the Peak Displacements of Different Shock Absorbing Bearings under the Action of 0.4PGA Seismic Wave

Structural vibration response parameters	El centro M2	El centro M3	Taft M2	Taft M3	1979 M2	1979 M3
x	49.7%	13.4%	59.6%	29.4%	51.8%	20.4%
y	37.9%	15.8%	59.5%	19.5%	44.9%	25.3%
z	53.9%	19.4%	62.6%	35.7%	61.4%	30.8%

Acceleration comparison analysis of key nodes

The comparative analysis of the acceleration reduction effects under the action of 0.4g seismic waves on U-shaped rubber composite seismic isolation bearings and lead-core rubber bearings is shown in Figure 8, which presents the key node acceleration time-history curves for three directions under three types of seismic waves for both the U-shaped rubber composite seismic isolation reticulated shell structure and the lead-core rubber seismic isolation reticulated shell structure. Figure 9 shows the peak node acceleration in three directions under the same three types of seismic waves. Table 5 provides the vibration reduction rates for the U-shaped rubber composite seismic isolation bearing and the lead-core rubber bearing. It can be seen from these results:

The two types of seismic isolation bearings have the effect of reducing the peak nodal acceleration of the reticulated shell structure. The U-shaped rubber composite seismic isolation bearing has the damping rate of 41.1%,49.5% and 53.1% in the X, Y and Z directions under El centro wave, 55.0%,54.3% and 74.3% under Taft wave, and 71.7%,73.7% and 77.6% under 1979 wave; the lead core rubber bearing has the damping rate of 34.3%,18.4% and 46.9% in the X, Y and Z directions under El centro wave, 54.8%,45.9% and 57.2% under Taft wave, and 46.2%,38.6% and 53.8% under 1979 wave.

It can be seen that the displacement reduction effect of the two types has improved. Under the influence of three seismic waves, the peak Z-direction nodal acceleration of both uncontrolled and controlled structures is greater than that in the X and Y directions. The two types of seismic isolation bearings show significant vibration reduction under the Taft wave and 1979 wave. Moreover, compared to the unreinforced reticulated shell structure, the horizontal vibration reduction rate of the two types of seismic isolation reticulated shells is lower than their vertical vibration reduction rate.

Compared to the lead-core rubber bearing, the difference in vibration reduction rate under El centro-wave action is between 6.8% and 31.1%, under Taft-wave action it is between 0.2% and 17.1%, and under 1979-wave action it is 23.8-35.2%. Under 1979-wave action, the difference in vibration reduction rate is significant, with the U-shaped rubber composite seismic isolation bearing showing superior acceleration reduction performance.

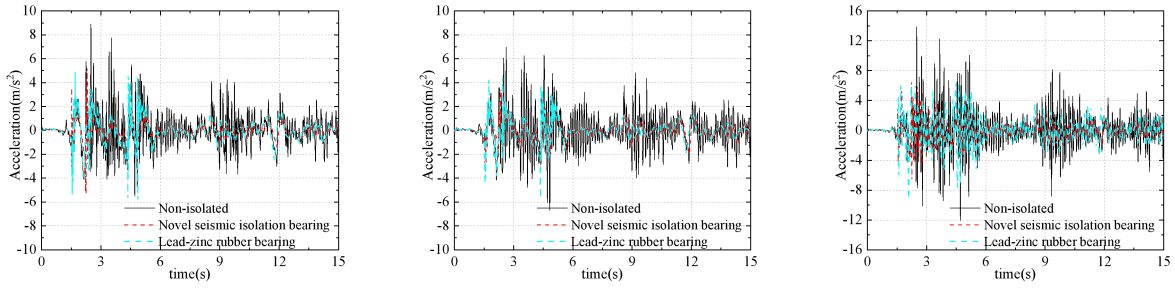

(a) El centro-X **(b) El centro-Y** **(c) El centro-Z**

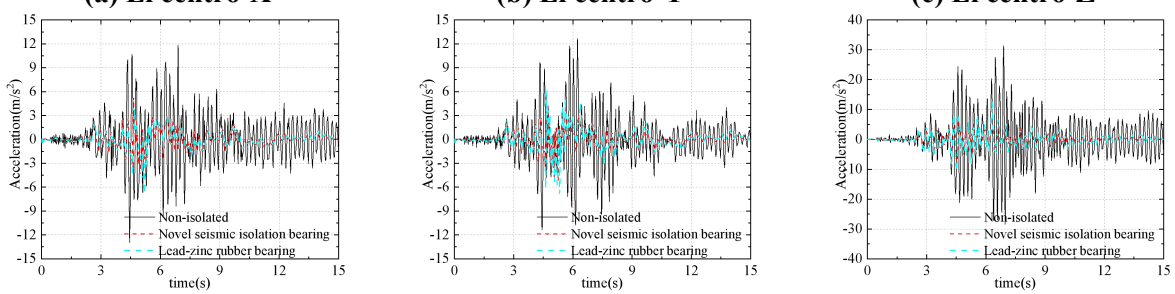

(d) Taft-X **(e) Taft-Y** **(f) Taft-Z**

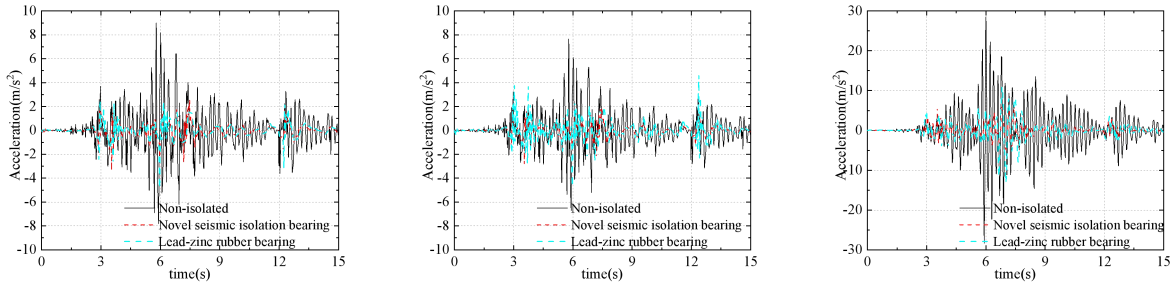

(g) 1979-X (h) 1979-Y (i) 1979-Z

Figure 8. Acceleration Time History Curve of Key Nodes of the Latticed Shell Structure under the Action of 0.4PGA Seismic Wave

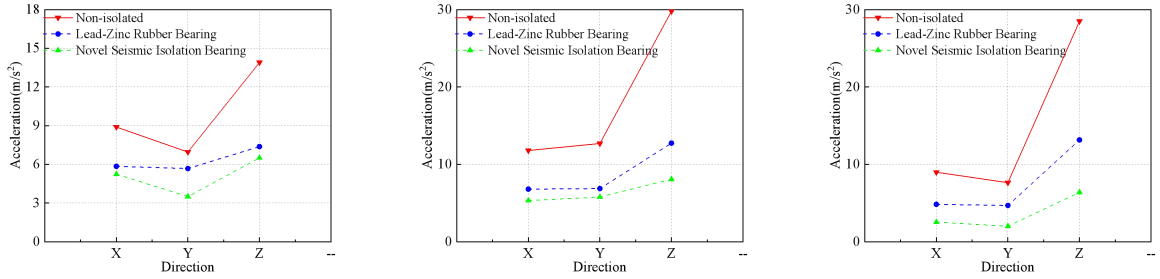

(a) El centro (b) Taft (c) 1979

Figure 9. Peak Acceleration of Key Nodes of the Latticed Shell Structure under the Action of 0.4PGA Seismic Wave

Table 5. Comparison of the Shock Absorption Rates of the Acceleration Peaks of Different Shock-Absorbing Bearings under the Action of 0.4PGA Seismic Wave

Structural vibration response parameters	El centro M2	El centro M3	Taft M2	Taft M3	1979 M2	1979 M3
x	41.1%	34.3%	55.0%	54.8%	71.7%	46.2%
y	49.5%	18.4%	54.3%	45.9%	73.7%	38.6%
z	53.1%	46.9%	74.3%	57.2%	77.6%	53.8%

Comparison analysis of internal forces in members

The comparative analysis of the seismic energy reduction effects under the action of 0.4g seismic waves on U-shaped rubber composite base bearings and lead-core rubber base bearing members is shown in Figure 10, which presents the time-history curves of internal forces in the members for both U-shaped composite rubber seismic isolation reticulated shell structures and lead-core rubber seismic isolation reticulated shell structures under three types of seismic waves. Table 6 provides the seismic reduction rates of the reticulated shell members using U-shaped rubber composite seismic isolation base bearings. It can be seen from this that:

Two types of seismic isolation bearings have vibration-damping effects on the peak internal forces of the truss members in the reticulated shell structure. The U-shaped rubber composite seismic isolation bearing has a vibration damping rate of 47.1% for El centro-waves, 62.2% for Taft waves, and 66.8% for 1979 waves; the lead-core rubber bearing has vibration damping rates of 35.1% in the X, Y, and Z directions for El centro-waves, 58.9% for Taft waves, and 47.5% for 1979 waves. Both types of seismic isolation bearings show significant vibration damping effects on the internal forces of the truss members under Taft waves and 1979 waves.

Compared to the lead-core rubber bearing, the difference in seismic reduction rate for internal forces in members under El centro-wave action is 12.0%, under Taft-wave action it is 3.3%, and under 1979-wave action it is 19.3%. Under 1979-wave action, the difference in seismic reduction rate is significant, indicating that the U-shaped rubber composite seismic isolation bearing has superior performance in reducing internal forces in members. This demonstrates that using the U-shaped rubber composite seismic isolation bearing can effectively reduce the peak internal forces in members of reticulated shell structures under seismic loads.

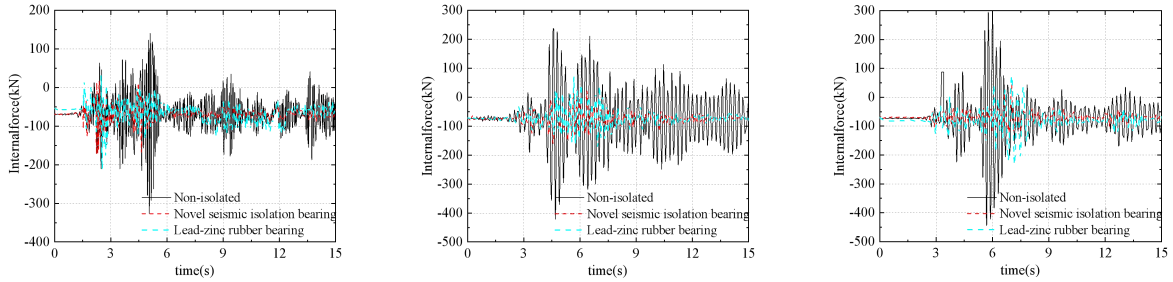

(a) 1979-X **(b) 1979-Y** **(c) 1979-Z**

Figure 10. Internal Force Time History Curve of Key Members of the Latticed Shell Structure under the Action of 0.4PGA Seismic Wave

Table 6. Comparison of the Shock Absorption Rates of the Peak Internal Forces of the Members of Different Shock-Absorbing Bearings under the Action of 0.4PGA Seismic Wave

El centro M2	El centro M3	Taft M2	Taft M3	1979 M2	1979 M3
47.1%	35.1%	62.2%	58.9%	66.8%	47.5%

6. Comparative Analysis of Seismic Isolation Effect of U-Shaped Rubber Composite Seismic Isolation Bearings under Different PGA Effects

Comparison and analysis of key node displacement

The seismic response of U-shaped rubber composite base isolated bearings under 0.2g and 0.4g seismic waves is compared. The isolation effect under 0.4g seismic waves has been illustrated in Section 3.5, so it will not be repeated here. Figure 11 shows the key node displacement time histories in three directions under three different 0.2g seismic wave conditions. Figure 12 presents the peak node displacements in three directions under the same three 0.2g seismic wave conditions. Table 7 provides a comparison table of the damping ratios for 0.2g and 0.4g seismic waves. From this, we can see:

The U-shaped rubber composite seismic isolation bearings have damping rates of 8.4%,5.0%, and 41.1% in the X, Y, and Z directions under a 0.2gEl centro wave, 32.6%,26.2%, and 58.7% under a 0.2gTaft wave, and 26.3%,15.4%, and 56.6% under the 1979 wave. Similar to the 0.4g earthquake wave, the damping rate in the Z direction remains higher than that in the X and Y directions, with more significant damping observed under the Taft and 1979 waves, while the damping effect is minimal in the X and Y directions under the El centro wave.

Compared to the 0.4g seismic wave, the El centro-wave displacement damping rate differs by 12.8% to 41.3%, the Taft wave by 3.9% to 33.3%, and the 1979 wave by 4.8% to 29.5%. This is because under major earthquakes, seismic isolation bearings can absorb and dissipate seismic energy through greater plastic deformation, significantly reducing the dynamic response of structures. Under minor earthquakes, the plastic deformation of structures is smaller, and the seismic isolation bearings either do not enter plasticity or enter it for a shorter period. Therefore, this energy dissipation mechanism makes the seismic isolation system exhibit superior damping performance under major earthquakes.

Acceleration comparison analysis of key nodes

The comparative analysis of the seismic acceleration reduction effects under 0.2g and 0.4g seismic waves on U-shaped rubber composite base isolation bearings is presented. Figure 13 shows the key node acceleration time history curves in three directions under three 0.2g seismic wave conditions, while Figure 14 presents the peak node acceleration in three directions under the same three 0.2g seismic wave conditions. Table 8 provides a comparison table of the vibration reduction rates under 0.2g and 0.4g seismic waves, from which it can be seen:

The seismic isolation rate of U-shaped rubber composite seismic isolation bearings in the X, Y and Z directions is 11.4%,14.9% and 41.9% under the action of 0.2gEl centro wave, 40.0%,30.9% and 51.4% under the action of 0.2gTaft wave, and 43.7%,48.0% and 68.3% under the action of 1979 wave. The seismic isolation rate in the Z direction is still higher than that in the X and Y directions, and the seismic isolation is more obvious under the action of Taft wave and 1979 wave.

Compared to the 0.4g seismic wave, the El

centro-wave acceleration damping rate differs by 11.2% to 34.6%, the Taft wave by 15.0% to 23.4%, and the 1979 wave by 9.3% to 28.0%. This indicates that as PGA increases, the acceleration damping rate changes similarly to the displacement damping rate, gradually increasing, with vertical damping performance being better than horizontal bidirectional damping performance.

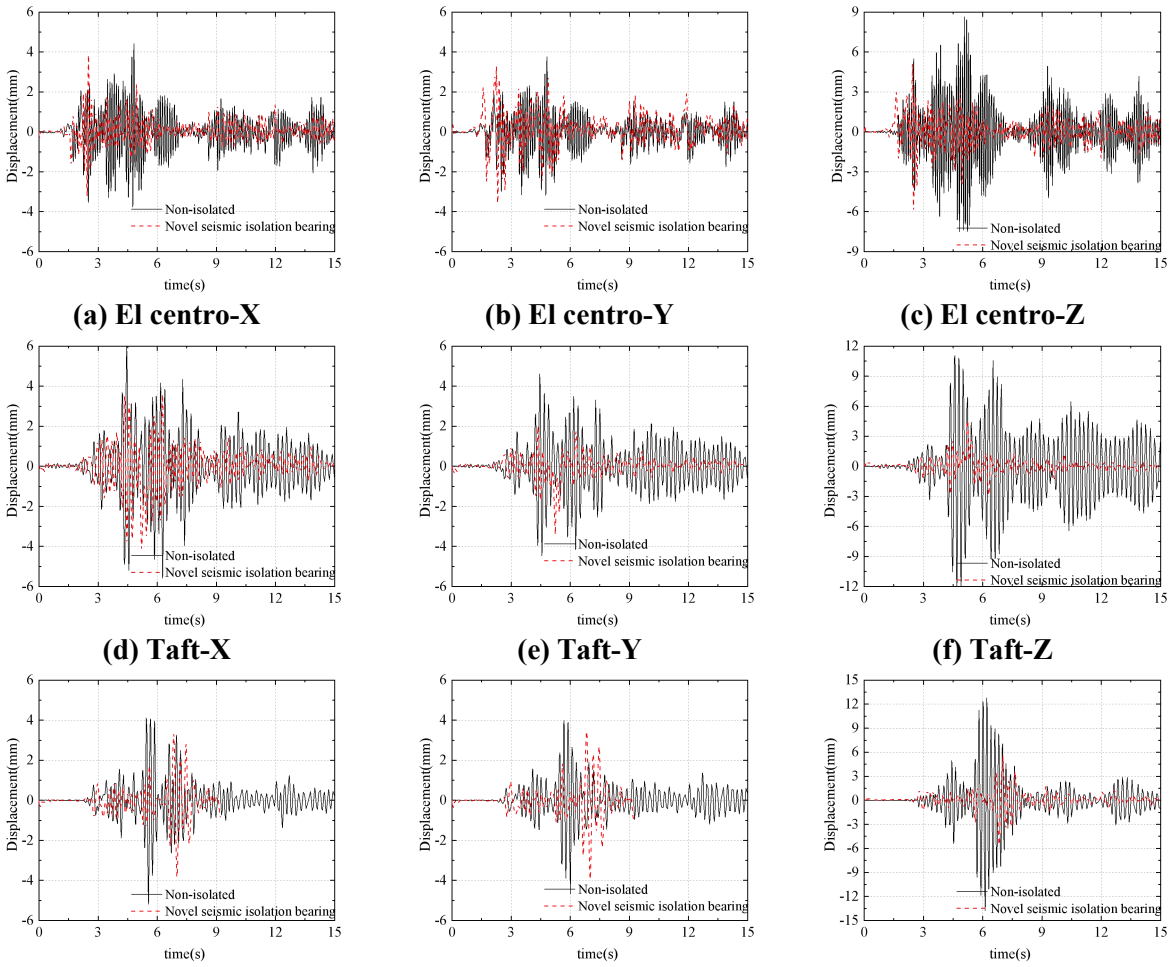

(a) El centro-X (b) El centro-Y (c) El centro-Z

(d) Taft-X (e) Taft-Y (f) Taft-Z

(g) 1979-X (h) 1979-Y (i) 1979-Z

Figure 11. Displacement Time History Curve of Key Nodes under the Action of 0.2PGA Seismic Wave

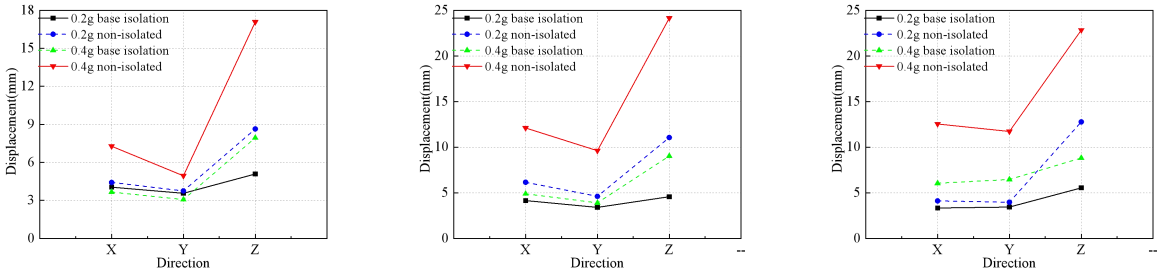

(a) El centro (b) Taft (c) 1979

Figure 12. Peak Displacement of Key Nodes of the Latticed Shell Structure under the Action of 0.2PGA Seismic Wave

Table 7. Comparison of Shock Absorption Rates of Displacement Peaks under Different PGAs

Structural vibration response parameters	Elcentro 0.4g	Elcentro 0.2g	Taft 0.4g	Taft 0.2g	1979 0.4g	1979 0.2g
x	49.7%	8.4%	59.6%	32.6%	51.8%	26.3%
y	37.9%	5.0%	59.5%	26.2%	44.9%	15.4%
z	53.9%	41.1%	62.6%	58.7%	61.4%	56.6%

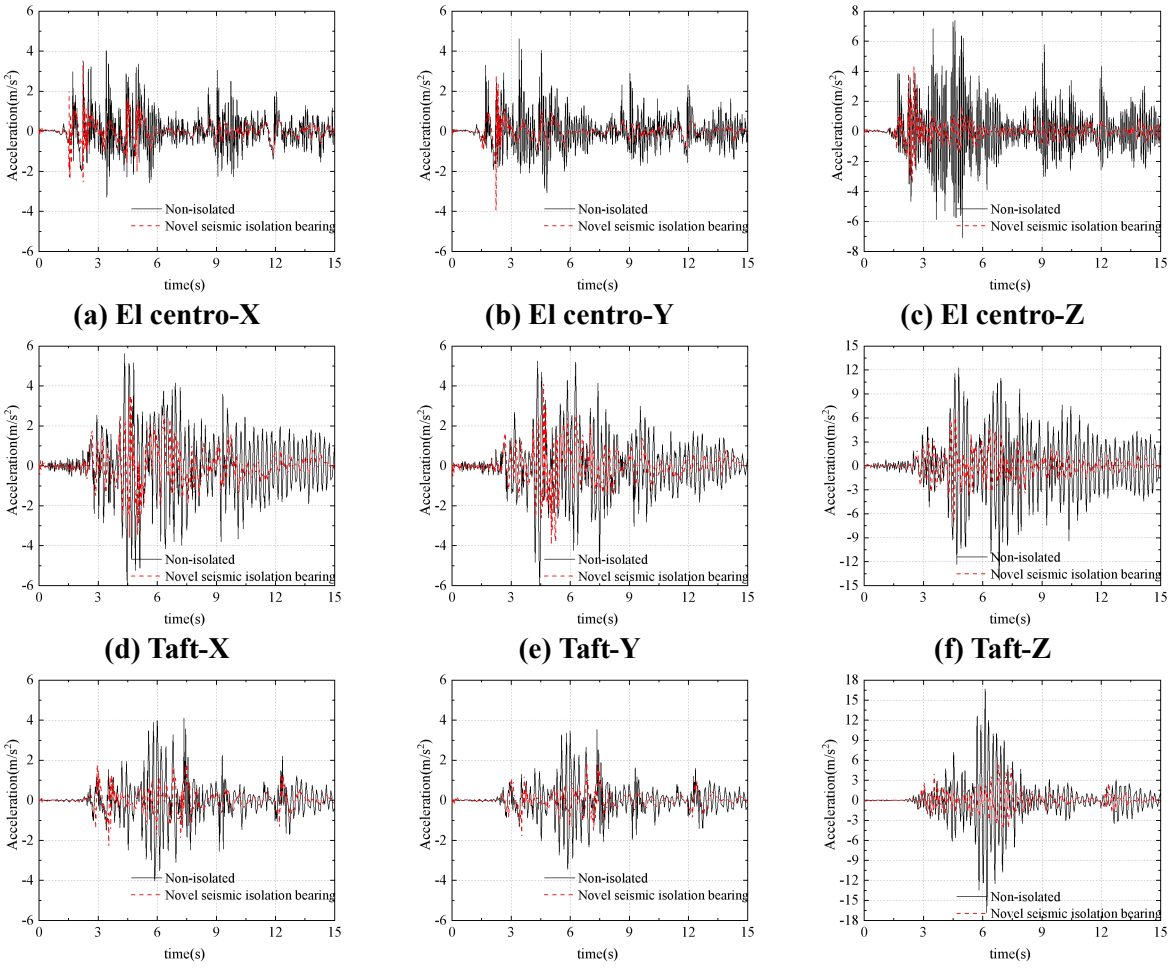

(a) El centro-X (b) El centro-Y (c) El centro-Z

(d) Taft-X (e) Taft-Y (f) Taft-Z

(g) 1979-X (h) 1979-Y (i) 1979-Z

Figure 13. Acceleration Time History Curve of Key Nodes of the Latticed Shell Structure under the Action of 0.2PGA Seismic Wave

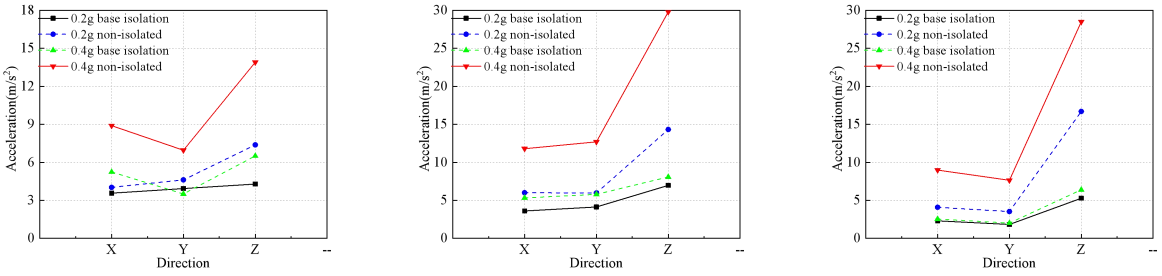

(a) El centro (b) Taft (c) 1979

Figure 14. Peak Acceleration of Key Nodes of the Latticed Shell Structure under the Action of 0.2PGA Seismic Wave

Table 8. Comparison of Shock Absorption Rates of Acceleration Peaks under Different PGAs

Structural vibration response parameters	El centro 0.4g	El centro 0.2g	Taft 0.4g	Taft 0.2g	1979 0.4g	1979 0.2g
x	41.1%	11.4%	55.0%	40.0%	71.7%	43.7%
y	49.5%	14.9%	54.3%	30.9%	73.7%	48.0%
z	53.1%	41.9%	74.3%	51.4%	77.6%	68.3%

Comparison analysis of internal forces in members

The displacement and vibration damping effects of U-shaped rubber composite seismic isolation bearings under 0.2g and 0.4g seismic waves are compared and analyzed. Figure 15 shows the time-history curves of internal forces in the members under three 0.2g seismic waves, and

the table shows the vibration damping rate of the reticulated shell members with U-shaped rubber composite seismic isolation bearings. It can be seen from the figure that:

The seismic reduction rate of the U-shaped rubber composite isolation bearing is 36.7% under El centro wave, 48.4% under Taft wave and 46.3% under 1979 wave.

Compared with 0.4g seismic wave, the internal force damping rate of El centro wave member is 10.4% different, the damping rate of Taft wave is 13.8% different, and the damping rate of 1979 wave is 20.5% different. This indicates that with the increase of PGA, the internal force damping rate of the member increases, and this seismic isolation bearing is more suitable for large earthquakes.

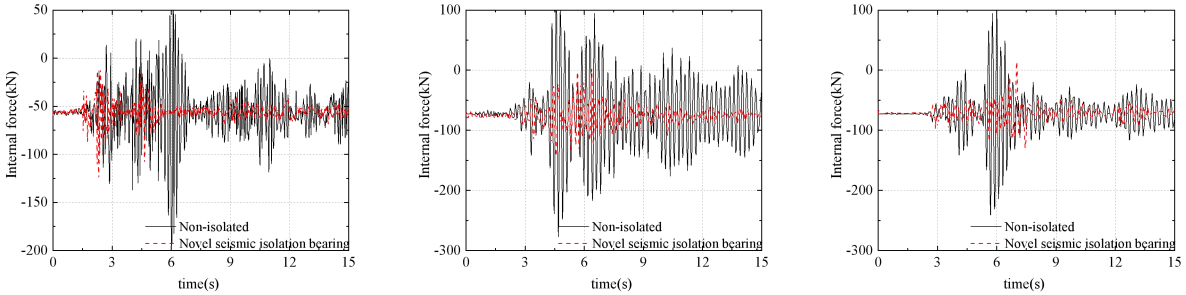

(a) 1979-X **(b) 1979-Y** **(c) 1979-Z**

Figure 15. Internal Force Time History Curve of Key Members of the Latticed Shell Structure under the Action of 0.2PGA Seismic Wave

Table 9. Comparison of the Shock Absorption Rates of the Peak Internal Forces of the Members under Different PGAs

El centro M2	El centro M3	Taft M2	Taft M3	1979 M2	1979 M3
47.1%	36.7%	62.2%	48.4%	66.8%	46.3%

7. Conclusion

This chapter combines the U-shaped composite damper proposed in Chapter Two with lead rubber bearings to form a U-shaped rubber composite seismic isolation bearing, which is then applied to the reticulated shell structure. By comparing the vibration reduction effects of the U-shaped rubber composite seismic isolation bearing with those of the lead rubber bearing, and by comparing the vibration reduction effects of the U-shaped rubber composite seismic isolation bearing under different PGA earthquake intensities, the following rules have been obtained:

(1) The first period of the reticulated shell structure with U-shaped rubber composite seismic isolation bearings is 1.35s, which is 6.75 times that of the uncontrolled structure and 2.14 times that of the reticulated shell structure with lead rubber bearings. It effectively extends the natural vibration period of the structure and thus reduces the seismic response of the structure.

(2) Under the influence of different seismic waves, the peak displacement, acceleration, and internal force reduction effects of nodal seismic isolation supports in reticulated shell structures using U-shaped rubber composite bearings are all better than those of lead-core rubber bearings, with maximum differences of 40%,35.2%, and 19.3%, respectively; the seismic isolation effects of the two types of bearings under the 1979 wave and Taft wave are superior to those under the El centro wave, and their Z-direction displacement and acceleration reduction effects are better than those in the X and Y directions.

(3) Under the action of a 0.4g seismic wave, the nodal peak displacement, acceleration, and internal force reduction effects of the U-shaped rubber composite base isolated truss structure are all better than those under a 0.2g seismic wave, with maximum differences of 41.3%,34.6%, and 20.5%, respectively. Therefore, the U-shaped rubber composite base isolated truss system exhibits superior seismic performance under major earthquake conditions.

References

[1] Du Xinxi. Design and Analysis of Large Span Spatial Structures [M]. Beijing: China Architecture & Building Press, 2014.

[2] Cao Zi, Xue Suduo. Science Press [M]. Beijing: 2005.

[3] Ma Jinfeng, Liu Mingjie. Study on vibration control of String-supported dome structure with damping rod replacement [J]. Vibration

and Shock, 2024,43(18):173-185.
[4] Zhao Xiang, Liu Zhonghua, Wang Sheliang, et al. Seismic control analysis of large-span spatial structures under multidimensional seismic action [J]. Journal of Seismic Engineering, 2018,40(03): 398-405.
[5] Zhuang Peng, Wang Wenting, Han Miao, et al. Study on the vibration damping effect of friction-SMA spring composite energy dissipation support in the surrounding single-layer spherical reticulated shell structure [J]. Journal of Vibration and Shock, 2018,37(04):99-109.
[6] Zhu Limin, Xue Yantao, Tang Rongwei. Application of Lightly Flexible Constrained Supports in Large Span Spatial Structures [J]. Architectural Structure, 2015,45(11):18-21.
[7] Ma Yongquan, Qiu Hongxing. Three-dimensional seismic isolation control for seismic response of a curved roof with a string support [J]. Journal of Hunan University (Natural Science Edition), 2013,40(12):21-30.
[8] YONG-CHUL K, XUE S, ZHUANG P, YONG-CHUL K, XUE S, ZHUANG P, et al. Seismic isolation analysis of FPS bearings in spatial lattice shell structures [J]. Earthquake Engineering and Engineering Vibration, 2010,9 (1): 93-102.
[9] Zhuang Peng, Ji Guangyu, Liu Pei, et al. Seismic response analysis of single-layer spherical reticulated shell structures with multi-functional friction pendulum system [J]. Vibration and Shock, 2020,39(08):79-87.
[10] KONG D, WANG L, WU L, KONG D, WANG L, WU L, et al. Influence of column supports on seismic performance of K8 single-layer spherical reticulated domes with friction pendulum bearings[J]. International Journal of Steel Structures, 2019,19: 879-887.
[11] ZHANG C, NIE G, DAI J, ZHANG C, NIE G, DAI J, et al. Seismic isolation research on a double-layer lattice structure using shaking table tests[J]. International Journal of Steel Structures, 2019,19: 1237-1248.
[12] Zhu Zhaochen, Luo Yongfeng, Liu Yipeng, et al. Vibration control test of single-layer spherical reticulated shell MTMD [J]. Journal of Southeast University (Natural Science Edition), 2019,49(04):696-704.
[13] Han Xi. Research on the Dynamic Response of the Overhead Frame Structure with Three-Dimensional Isolation Friction Pendulum for Subway [D]. Xi'an University of Architecture and Technology, 2023.

